ACS APPLIED MATERIALS & INTERFACES

Research Article

www.acsami.org

Novel Pyrolyzed Polyaniline-Grafted Silicon Nanoparticles Encapsulated in Graphene Sheets As Li-Ion Battery Anodes

Zhe-Fei Li,[†] Hangyu Zhang,[‡] Qi Liu,[†] Yadong Liu,[†] Lia Stanciu,[‡,§] and Jian Xie*,[†]

[†]Department of Mechanical Engineering, Indiana University−Purdue University Indianapolis, Indianapolis, Indiana 46202, United States

[‡]Weldon School of Biomedical Engineering, Purdue University, West Lafayette, Indiana 47907, United States

[§]School of Materials Engineering, Purdue University, West Lafayette, Indiana 47907, United States

Supporting Information

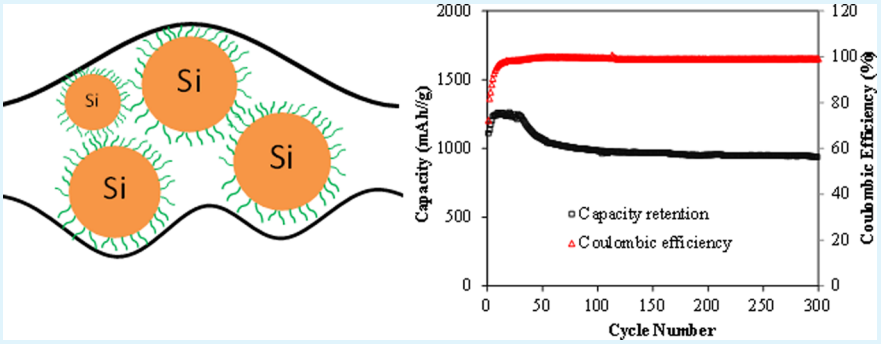

ABSTRACT: A simple method to fabricate graphene-encapsulated pyrolyzed polyaniline-grafted Si nanoparticles has been developed. Instead of using Si nanoparticles with a native oxide layer, HF-treated Si nanoparticles were employed in this work. The uniqueness of this method is that, first, a PANI layer over the Si nanoparticles was formed via the surface-initiated polymerization of aniline on the surface of aniline-functionalized Si nanoparticles; then, the PANI-grafted Si nanoparticles were wrapped by the GO sheets via $\pi-\pi$ interaction and electrostatic attraction between the GO and the PANI. Finally, the GO and PANI were pyrolyzed, and this pyrolyzed PANI layer tightly binds the graphene sheets and the Si nanoparticles together in the composite. The composite materials exhibit better cycling stability and Coulombic efficiency as anodes in lithium ion batteries, as compared to pure Si nanoparticles and physically mixed graphene/Si composites. After 300 cycles at a current density of 2 A/g, the composite electrodes can still deliver a specific capacity of about 900 mAh/g, which corresponds to ~76% capacity retention. The enhanced performance can be attributed to the absence of surface oxides, the better electronic conductivity, faster ion diffusion rate, and the strong interaction between the graphene sheets and the tightly bound carbon-coated Si nanoparticles.

KEYWORDS: *graphene, silicon, polyaniline, surface-initiated polymerization, diazonium functionalization, lithium-ion batteries*

1. INTRODUCTION

Driven by the rapidly growing field of hybrid and electric vehicles, there is increasing demand for lithium-ion batteries (LIBs) with high energy density, long cycle life, and low cost. One of the most widely used anode materials in LIBs, graphite, possesses a theoretical specific capacity of only about 370 mAh/g, limiting the specific energy of LIBs.[1] Recently, silicon (Si) has been regarded as one of the most promising anode materials for high-performance LIBs, due to its exceptionally high specific capacity (>4200 mAh/g).[2] However, Si suffers from several issues, i.e. relatively low conductivity, >300% volume change upon lithium-ion insertion/deinsertion in Si, and rapid capacity fade.[3] Among these issues, the dramatic volume change can result in the pulverization of the Si particles, consequently causing a loss of the electrical contact with the conductive additives and between the Si particles, and an unstable solid electrolyte interphase (SEI) layer.[4,5] To overcome these disadvantages, various nanostructured Si materials have been developed, including Si nanoparticles,[6] nanoporous Si,[7] nanowires,[8] core−shell structures,[9,10] nanotubes,[11] Si/carbon nanocomposites,[12−15] covalently bonded Si/carbon nanotube composites,[16] and Si conformed in a conducting hydrogel.[17]

Recently, graphene/Si composite materials have been extensively studied by encapsulating Si nanoparticles within graphene nanosheets to create empty space to accommodate the volume change, buffer the mechanical stress, and improve the electrical conductivity. Graphene/Si composites can be prepared by drying an aqueous suspension of Si nanoparticles and graphene oxide (GO) and then thermally reducing the

Received: February 28, 2014
Accepted: April 4, 2014
Published: April 4, 2014

Scheme 1. Schematic Illustration of Synthetic Procedure of Graphene/C/Si Composites

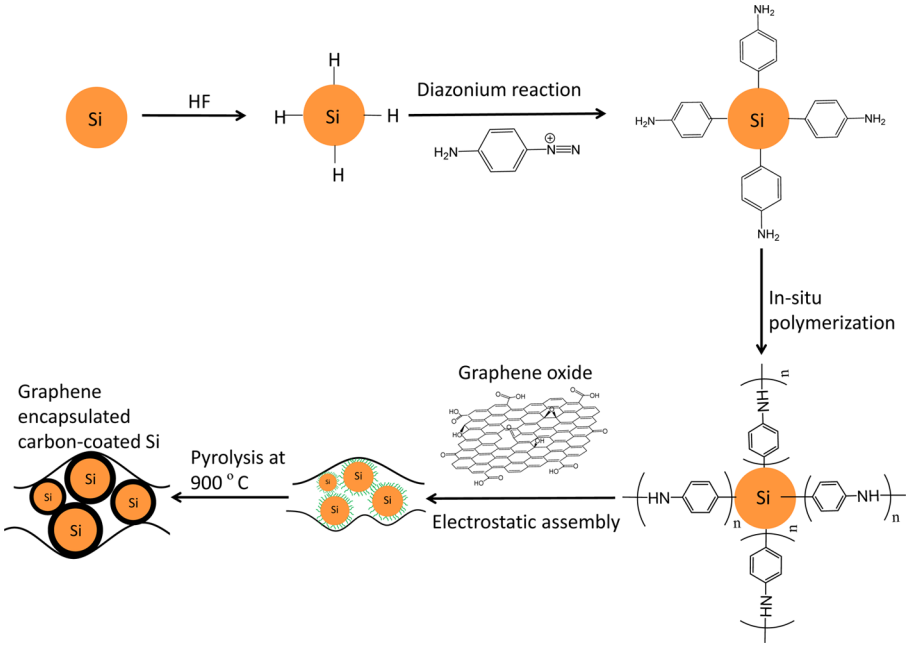

GO.[18−21] The challenge of developing a uniform graphene/Si composite lies in the Si nanoparticles tending to aggregate in the aqueous solution, resulting in the inhomogeneous mixing of GO and Si. Creating an oxide layer on the Si nanoparticles and further functionalizing the Si nanoparticles to enhance their dispersion and the interaction between GO and Si can result in more uniform graphene/Si composites. For example, graphene-bonded Si nanocomposites prepared using aminopropyltriethoxysilane-functionalized Si nanoparticles instead of conventional Si nanoparticles showed good performance as anodes in LIBs.[22] However, the SiO_2 layer, both an electrical insulator and a Li^+ diffusion barrier, has a negative impact on the electrochemical performance of Si-based electrodes (i.e., lower reversible capacity and Coulombic efficiency).[23−25] Thus, the use of an oxide (i.e., SiO_2) layer seems to create a dilemma. On one hand, the oxide layer helps to improve the dispersion; on the other hand, it may decrease the performance, which hinders the preparation of uniform graphene-encapsulated Si composites without a SiO_2 passivation layer. Here, we report a facile route to prepare graphene-encapsulated pyrolyzed polyaniline (PANI)-grafted Si nanoparticles without an oxide layer, which exhibited excellent performance as LIB anodes (i.e., improved cycling stability and Coulombic efficiency).

2. EXPERIMENTAL SECTION

2.1. Synthesis of GO. The GO was prepared following the procedures reported in our previous work.[26] Natural graphite flakes were preoxidized before oxidation by Hummers' method. Two grams of preoxidized graphite, 1 g of sodium nitrate, and 46 mL of sulfuric acid were mixed and stirred for 15 min in a 500 mL flask immersed in an ice bath. Then 6 g of potassium permanganate was slowly added to the above suspension solution. After 15 min, the temperature was heated up to 35 °C and maintained at that temperature for 30 min. A total of 92 mL of water was then added slowly to the suspension, causing a violent effervescence. The temperature was maintained at about 98 °C for 30 min. The suspension was diluted by 280 mL of water and treated with 10 mL of 30% H_2O_2 to reduce the unreacted potassium permanganate. Finally, the GO was washed successively with 1 M HCl solution and DI water by centrifugation several times to remove residual salts and acid. The obtained graphite oxide was sonicated to achieve a stable GO dispersion in water. Then, the GO dispersion solution was subjected to another centrifugation at 5000 rpm for 5 min to remove the unexfoliated GO. The purified GO was diluted in DI water to a concentration of 1 mg/mL.

2.2. Diazonium Functionalization of Si. Si nanoparticles (<50 nm, Alfa Aesar) were first treated with 10% HF to remove the surface oxides under a N_2 atmosphere and, then, stored in an Ar-filled glovebox before use. HF-treated Si, p-phenylenediamine, and H_2SO_4 were dispersed in the N_2-purged DI water. The dispersion was constantly stirred and kept in an ice bath. A solution containing $NaNO_2$ was added dropwise into the above dispersion. The dispersion was then vigorously stirred at room temperature for 4 h under a N_2 atmosphere. The resulting aniline-functionalized Si was filtrated with a 0.025 μm filter membrane, washed with DI water and ethanol, and vacuum-dried.

2.3. In Situ Polymerization of Aniline on Functionalized Si. The aniline-functionalized Si, aniline monomer, and HCl were dispersed in DI water. A solution of the oxidant, $(NH_4)_2S_2O_8$ (APS), was rapidly added into the above dispersion. The mixture was stirred for 24 h, and the product was filtered, washed, and vacuum-dried.

2.4. Preparation of Graphene-Encapsulated Pyrolyzed PANI-Grafted Si Nanoparticles. A GO aqueous dispersion and a PANI-grafted Si nanoparticle dispersion were mixed, sonicated, and stirred for 4 h. The mixture was filtrated and freeze-dried. Finally, the graphene-encapsulated carbon-coated Si composites were yielded by carbonization at 900 °C for 2 h at a heating rate of 2 °C/min under an argon atmosphere.

2.5. Characterization. Raman spectra were taken by a Craic Tech spectrometer with laser excitation at 785 nm. X-ray photoelectron spectroscopy (XPS) was carried out on a Kratos AXIS Ultra X-ray photoelectron spectrometer. Thermal gravimetric analysis (TGA) curves were obtained using the TA Instrument SDT Q600. The morphology was characterized by a Philips CM 200 transmission electron microscope (TEM) and a Hitachi SU-70 scanning electron microscope (SEM). The N_2 adsorption/desorption isotherms were measured by a Quantachrome Autosorb-iQ analyzer at 77 K. The Brunauer−Emmett−Teller (BET) specific surface area was calculated using adsorption data at the relative pressure range of 0.05−0.3. The total pore volumes were estimated from the amount adsorbed at a

relative pressure (P/P_0) of 0.99. The BJH pore size distribution was calculated based on the desorption branch of the isotherm.

2.6. Electrode Fabrication and Electrochemical Test. The electrochemical tests were measured in a 2016R-type coin cell. Lithium foil was used as the counter electrode. The working electrode was fabricated by pasting the slurry containing 70% active materials, 15% SuperP, and 15% poly(acrylic acid) in water onto a Cu foil using the doctor-blade method. The electrode was then dried in a vacuum oven at 60 °C for 12 h and then assembled into the coin cell in an Ar-filled glovebox. The mass loading of the active material on each electrode was about 0.3 mg/cm^2. The electrolyte used was 1.2 M $LiPF_6$ in EC/EMC (3:7 v:v), and a Celgard polypropylene membrane was used as the separator. The galvanostatic charge/discharge tests were performed on an Arbin battery test station. Electrochemical impedance spectroscopy (EIS) was performed using the Solartron system (1287 + 1260).

3. RESULTS AND DISCUSSION

The strategy for uniformly encapsulating Si nanoparticles within graphene sheets through the electrostatic self-assembly method is depicted in Scheme 1. Si nanoparticles were first treated with 10% HF to remove the surface oxide and create H-terminated Si surfaces.[27] However, H-terminated Si nanoparticles are very hydrophobic and tend to form a surface oxide layer when exposed to air. In order to achieve a good aqueous dispersion of Si nanoparticles, H-terminated Si nanoparticles were functionalized with aniline groups via a diazonium reaction. Then, a thin polyaniline layer was formed over the surface of a Si nanoparticle by the *in situ* polymerization of aniline. This grafting method is similar to the surface-initiated polymerization that has been widely used to prepare polymer brushes on various surfaces.[28,29] When the GO dispersion and the PANI-grafted Si dispersion were mixed, a uniform dispersion was achieved. The presence of the thin PANI coating not only prevents the aggregation of Si nanoparticles but also has a strong interaction with GO due to the $\pi-\pi$ interaction and the electrostatic attraction between GO and PANI-grafted Si nanoparticles. Thus, the GO sheets were tightly bounded to the PANI-grafted Si nanoparticles. Then, these GO-wrapped PANI-grafted Si nanoparticles were heated at 900 °C in Ar to thermally reduce the GO into graphene and pyrolyze the PANI. The final composite has the unique feature that Si nanoparticles are wrapped by a covalently bonded carbon layer formed from the pyrolysis of the PANI and graphene sheets tightly bounded to the carbon layer. The additional thin carbon layer is expected to aid the electric conductivity between the Si nanoparticles and the graphene sheets and help constrain the volume expansion of Si nanoparticles.

SEM was carried out to examine the morphology of pyrolyzed graphene-encapsulated PANI-grafted Si, shown in Figure 1. It can be seen that the Si nanoparticles were well wrapped by the graphene sheets, indicating the uniform electrostatic assembly of GO and PANI-grafted Si nanoparticles. TEM was also employed to study the morphology of different Si samples. Pristine commercial Si nanoparticles typically have a particle size of 50−100 nm and a surface oxide layer several nanometers thick (Figure 2a). After the polymerization of aniline monomers on aniline-functionalized Si nanoparticles, a rough PANI layer with several nanometers thickness can be observed as the arrow indicates in Figure 2b. Figure 2c shows the TEM image of graphene-encapsulated pyrolyzed PANI-grafted Si nanoparticles, obtained by the thermal treatment of the self-assembled GO/PANI-grafted Si at

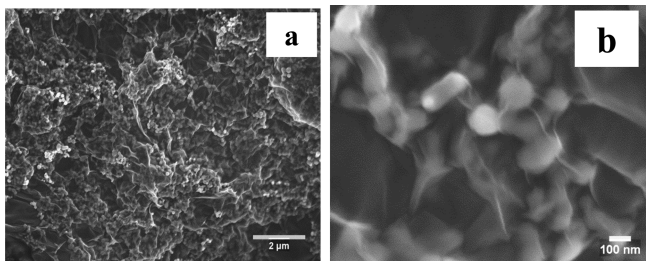

Figure 1. (a) Low resolution and (b) high resolution SEM images of graphene-encapsulated pyrolyzed PANI-grafted Si.

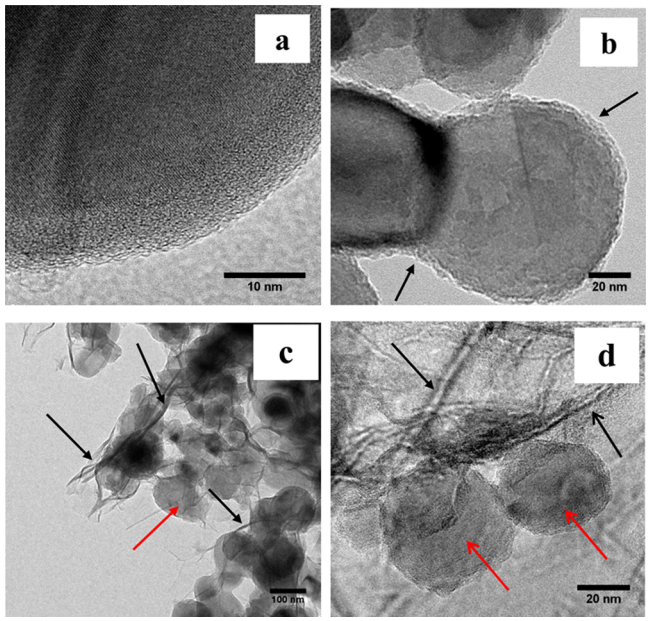

Figure 2. TEM images of (a) pristine Si nanoparticles, (b) PANI-Si (black arrows point to the PANI layer), and (c, d) graphene-encapsulated pyrolyzed PANI-grafted Si composites (Si nanoparticles, as the red arrows indicate; graphene sheet wrinkles, as the black arrows indicate).

900 °C in Ar. It can be clearly seen that the Si nanoparticles are wrapped in graphene sheets, consistent with SEM results. The high resolution TEM image (Figure 2d) provides a close view of the composites. Clearly, the Si nanoparticles were still coated with a rough layer, which is the pyrolyzed PANI (red arrows point to the pyrolyzed PANI-grafted Si, and black arrows point to the wrinkles of the graphene layer).

To understand the structural information on graphene-encapsulated pyrolyzed PANI-grafted Si, XPS and Raman spectroscopy were carried out. XPS spectra (N 1s) of pristine Si and aniline-functionalized Si were taken and are shown in Figure 3a. Compared to the absence of nitrogen element in pristine Si, weak N 1s peaks from the aminophenyl groups can be observed in the aniline-functionalized Si, indicating the successful grafting of aniline molecules on Si nanoparticles.[14] As can be seen in Figure 3b, the Raman spectrum of the Si nanoparticle displays a peak at around 520 cm^{-1}. Graphene exhibits two peaks at around 1590 cm^{-1} and about 1320 cm^{-1}, which can be ascribed to sp^2 carbons (G band) and the disordered aromatic structure of the sp^2 carbons (D band).[19] This disorder can be caused by surface defects, edges, or the formation of sp^3 bonds. The Raman spectrum of PANI-grafted Si shows the typical characteristic peaks of both Si and PANI

dx.doi.org/10.1021/am501239r | ACS Appl. Mater. Interfaces 2014, 6, 5996−6002

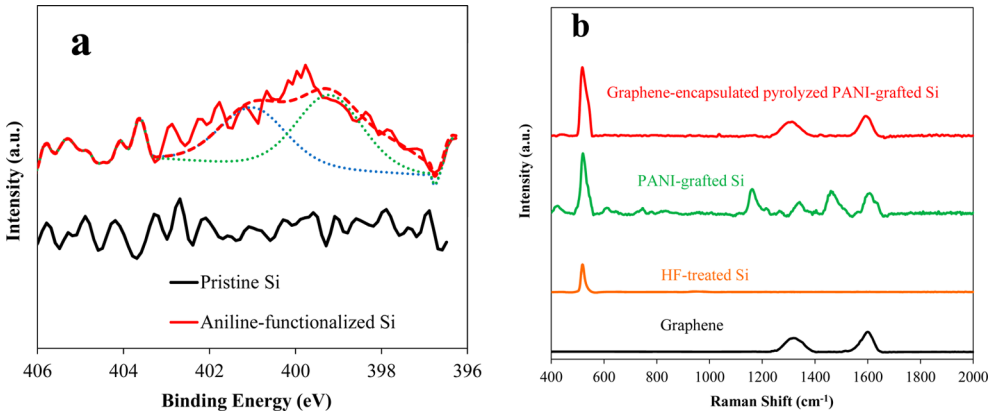

Figure 3. (a) XPS of pristine Si and aniline-functionalized Si and (b) Raman spectra of pristine Si, aniline-functionalized Si, PANI-grafted Si, and graphene-encapsulated pyrolyzed PANI-grafted Si.

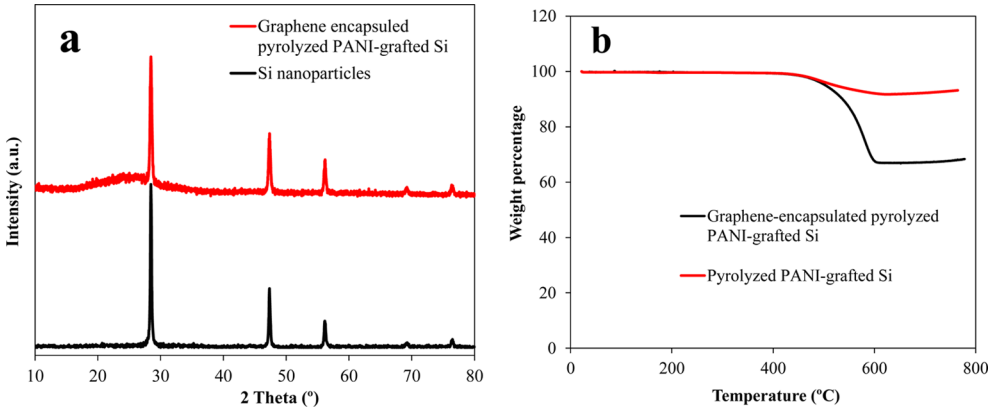

Figure 4. (a) XRD patterns of Si and graphene-encapsulated pyrolyzed PANI-grafted Si. (b) TGA curves of pyrolyzed PANI-grafted Si and graphene-encapsulated pyrolyzed PANI-grafted Si.

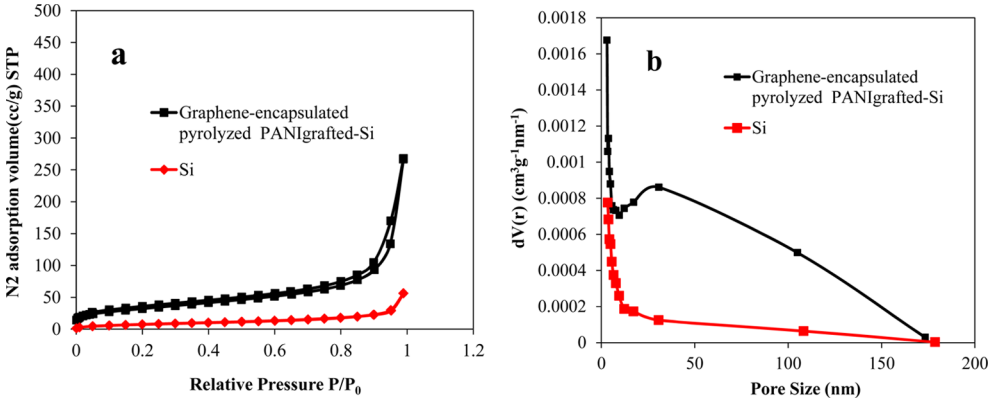

Figure 5. (a) N_2 adsorption−desorption isotherm and (b) BJH pore size distribution of Si and graphene-encapsulated pyrolyzed PANI-grafted Si.

(740, 1180, 1330, 1460, and 1592 cm^{-1}), indicating the successful grafting of PANI on the surface of the Si nanoparticles. In the graphene-encapsulated pyrolyzed PANI-grafted Si, the presence of graphene/carbon and Si are evidenced by three characteristic peaks around 520, 1320, and 1590 cm^{-1}. The PANI peak disappeared, suggesting that PANI has been pyrolyzed.

The X-ray diffraction (XRD) patterns of Si and graphene-encapsulated pyrolyzed PANI-grafted Si composites are shown in Figure 4a. The graphene-encapsulated pyrolyzed PANI-grafted Si composites exhibited the characteristic peaks of Si and a broad band around $2\theta = 25°$ of (002) diffraction peaks of graphene, which suggests that the graphene sheets exist in the composite. Combining the SEM, TEM, XPS, Raman, and XRD results, it is clear that the Si nanoparticles were wrapped by graphene sheets in the pyrolyzed PANI-grafted Si composite. From these results, it can be concluded that the synthesis depicted in Scheme 1 was carried out. Figure 4b displays the TGA curves of pyrolyzed PANI-grafted Si and graphene-encapsulated pyrolyzed PANI-grafted Si heated in air. A nearly 34% weight loss was recorded at 600 °C due to the decomposition of the carbon and graphene in the final composites. Thus, the weight percentage of Si in the final composites is about 66%. The weight loss of the pyrolyzed

dx.doi.org/10.1021/am501239r | ACS Appl. Mater. Interfaces 2014, 6, 5996−6002

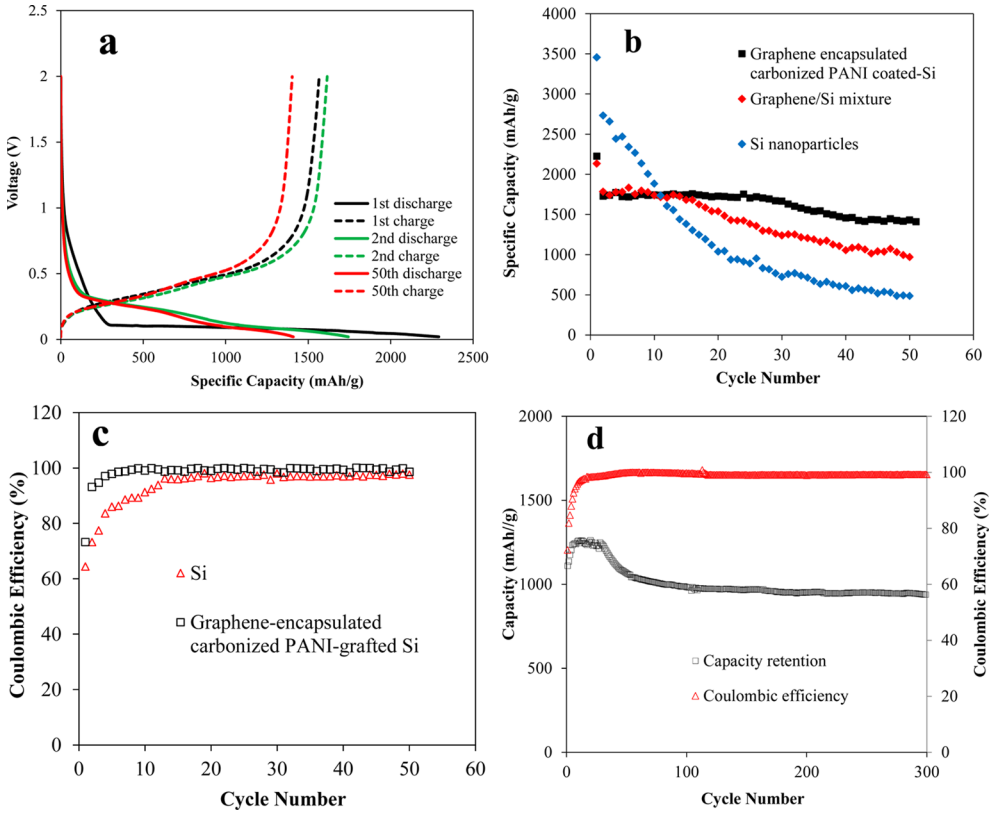

Figure 6. (a) Charge/discharge curves of the graphene-encapsulated pyrolyzed PANI-grafted Si. (b) Capacity retention and (c) Coulombic efficiency of the Si, graphene/Si mixture, and the graphene-encapsulated pyrolyzed PANI-grafted Si at a constant current density of 100 mA/g. (d) Capacity retention of the graphene-encapsulated pyrolyzed PANI-grafted Si at 2 A/g.

PANI-grafted Si sample at 600 °C is about 8%, suggesting that the carbon and graphene content in the composites were about 8% and 26%, respectively.

The porosity of the Si nanoparticles and the graphene-encapsulated pyrolyzed PANI-grafted Si composites was studied using N_2 adsorption−desorption isotherms at 77 K. The N_2 adsorption−desorption isotherms and the pore size distribution are shown in Figure 5. The pure Si nanoparticles showed a BET surface area of about 28 m^2/g and a pore volume of 0.087 cm^3/g. The BET surface area and pore volume of graphene-encapsulated pyrolyzed PANI-grafted Si composites was 131 m^2/g and 0.54 cm^3/g, respectively. The increase in the surface area and the pore volume of the composites is expected to facilitate the Li^+ ion transport and accommodate the volume expansion of Si nanoparticles during charging/discharging.

The electrochemical performance of the composites and the pristine Si nanoparticles was evaluated using galvanostatic charge/discharge cycles between 2−0.01 V. Figure 6a shows the galvanostatic charge/discharge curves (first, second, and 50th cycles) of graphene-encapsulated pyrolyzed PANI-grafted Si composites. The specific capacity is calculated based on the total mass of the active material (graphene/C and Si), and the cycling stability is shown in Figure 6b. The charge capacity of the pristine Si electrode rapidly decreased to less than 500 mAh/g after 50 cycles at a current density of 200 mA/g, due to the pulverization of the Si particles. In comparison, the graphene-encapsulated pyrolyzed PANI-grafted Si composites still retain a specific charge capacity of about 1400 mAh/g. It is worthwhile to point out that even if physically mixed graphene/Si composites still showed improved cycle performance compared to pure Si nanoparticles, there was a worse cycle life performance than that of the graphene-encapsulated pyrolyzed PANI-grafted Si composites. Interestingly, these physically mixed graphene/Si composites showed a similar cycle life behavior to that of the first 10 cycles of the graphene-encapsulated pyrolyzed PANI-grafted Si composites but then decayed rapidly as the pure Si nanoparticles do, which may be due to the loss of the contact between graphene and Si nanoparticles caused by volume expansion/shrinkage during long-term cycling. This demonstrates the advantage of the carbon layer on the Si nanoparticles (from the carbonization of the PANI layer on the Si nanoparticles) in the graphene-encapsulated pyrolyzed PANI-grafted Si composite. The physically mixed graphene sheets do not tightly bind the Si nanoparticles due to less of an interaction between the graphene sheets and the Si nanoparticles. Hence, they can improve the electric conductivity and buffer the volume change to a degree that is much better than that of pure Si nanoparticles in the first 10 cycles. However, without the pyrolyzed PANI layer on the Si nanoparticles, these graphene sheets cannot bind very tightly to the Si nanoparticles. Consequently, the capacity starts to decline rapidly after the 10th cycle, due to the pulverization of the Si nanoparticles and loss of electrical contact between graphene and Si.

To determine the exact capacity contributed by Si, graphene was tested as the anode in LIB. The initial capacity of graphene is about 800 mAh/g but quickly decays to below 300 mAh/g (Figure S3). Extracting the capacity contribution from graphene, the reversible capacity of the Si in composites can be estimated to be around 2000 mAh/g, which corresponds to about half of the theoretical capacity of Si. The Coulombic

dx.doi.org/10.1021/am501239r | ACS Appl. Mater. Interfaces 2014, 6, 5996−6002

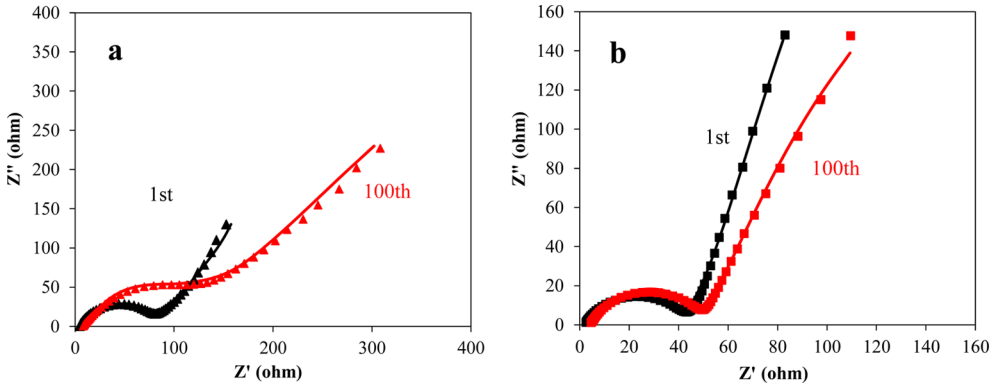

Figure 7. EIS spectroscopy of (a) Si and (b) graphene-encapsulated pyrolyzed PANI-grafted Si before and after 100 cycles.

efficiency was obtained by dividing the specific charge capacity by the specific discharge capacity. For the pristine Si, the first-cycle Coulombic efficiency was only 64.4% due to the initial SEI layer formation and irreversible lithium reaction with the surface oxides on the Si nanoparticles. For the graphene-encapsulated pyrolyzed PANI-grafted Si composites, the Coulombic efficiency for the first cycle was 73.2% (Figure 6c), which is comparable to the literature-reported values of MCMB anodes.[30] This is likely due to the irreversible lithium reaction with the residual functional groups on the graphene during the initial SEI layer formation. The Coulombic efficiency of the composites increased rapidly and remained above 99% during the following cycling tests, while the Coulombic efficiency of the pure Si nanoparticles increased slowly and stabilized around 98%. The lower Coulombic efficiency of pure Si is probably caused by the unstable SEI layer and the propagation of microdefects and electrically isolated areas within the anode, a result of the pulverization of the Si nanoparticle during cycling.[31] The high Coulombic efficiency of graphene-encapsulated pyrolyzed PANI-grafted Si composites is indicative of the excellent stability of the SEI layer, resulting from the uniform graphene wrapping of the Si nanoparticles and the aid of the surface carbon layer (from the PANI layer carbonization). To obtain long cycling results, charge/discharge tests at a current density of 2 A/g were carried out, shown in Figure 6d. Even after 300 cycles, the graphene-encapsulated pyrolyzed PANI-grafted Si composites still maintained a specific capacity above 900 mAh/g, which corresponds to 76% of initial capacity.

EIS measurements were conducted to understand the different electrochemical behaviors of Si and graphene-encapsulated pyrolyzed PANI-grafted Si composite electrodes, and the Nyquist plots are shown in Figure 7. A semicircle shape in the high frequency region and a straight line in the low frequency region can be observed. Figure 7a shows the Nyquist plots of the Si nanoparticle electrodes before and after 100 cycles. The semicircle became larger, suggesting that the charge transfer resistance increased, probably resulting from the pulverization of the Si nanoparticles and the thick SEI layer. In the graphene-encapsulated pyrolyzed PANI-grafted Si composites (Figure 7b), the semicircle became only slightly wider, a very small change. This suggests that the pulverization and agglomeration of the Si nanoparticles during cycling was effectively suppressed because the Si nanoparticles were wrapped in the carbon coating and graphene sheets. Thus, a stable SEI layer, fast electron transfer, and facile Li^+ diffusion path have been achieved, leading to the excellent cycling performance.

4. CONCLUSION

A novel synthesis has been developed to prepare surface-modified and oxide-free Si nanoparticles uniformly encapsulated within graphene sheets. The composites were synthesized by the *in situ* polymerization of aniline on aniline-functionalized Si nanoparticles, followed by the self-assembly with the Si nanoparticles because of a $\pi-\pi$ interaction and an electrostatic attraction between GO and PANI-grafted Si nanoparticles, and finally, their subsequent carbonization. The incorporation of graphene sheets to encapsulate the Si nanoparticles provides high electronic conductivity, high mechanical strength, and large pore volume to accommodate the volume expansion of the Si. As a result, compared to physically mixed graphene/Si composites and pure Si nanoparticles, the graphene-encapsulated pyrolyzed PANI-grafted Si composites exhibited enhanced electrochemical performance (i.e., cycling stability, rate performance, and Coulombic efficiency) as anodes in lithium-ion batteries. The composites can deliver a reversible specific capacity of ~1500 mAh/g (total mass of Si and graphene) at a charge/discharge rate of 50 mA/g and more than 900 mAh/g at 2 A/g. Even after 300 cycles at 2 A/g, the composites still can retain about 70% of the initial capacity. Further improving the synthetic conditions to control the relative mass ratio of Si/C/graphene and the electrode fabrication could lead to further improved electrochemical performance.

■ ASSOCIATED CONTENT

Ⓢ Supporting Information

Demonstration of aqueous dispersion of diazonium-functionalized Si nanoparticles; SEM and TEM images of graphene; electrochemical data of graphene electrodes. This material is available free of charge via the Internet at http://pubs.acs.org.

■ AUTHOR INFORMATION

Corresponding Author

*E-mail: jianxie@iupui.edu.

Notes

The authors declare no competing financial interest.

■ ACKNOWLEDGMENTS

This work was partially supported by the multidisciplinary Undergraduate Research Initiative (MURI) of Indiana University Purdue University Indianapolis (IUPUI). The

authors acknowledge Dr. Kateryna Artyushkova for the help in XPS experiments.

REFERENCES

(1) Tarascon, J. M.; Armand, M. Issues and Challenges Facing Rechargeable Lithium Batteries. *Nature* **2001**, *414*, 359−367.
(2) Poizot, P.; Laruelle, S.; Grugeon, S.; Dupont, L.; Tarascon, J. M. Searching for New Anode Materials for the Li-ion Technology: Time to Deviate From the Usual Path. *J. Power Sources* **2001**, *97*−*98*, 235−239.
(3) Zamfir, M. R.; Nguyen, H. T.; Moyen, E.; Lee, Y. H.; Pribat, D. Silicon Nanowires for Li-based Battery Anodes: A Review. *J. Mater. Chem. A* **2013**, *1*, 9566−9586.
(4) Li, H.; Huang, X.; Chen, L.; Wu, Z.; Liang, Y. A High Capacity Nano−Si Composite Anode Material for Lithium Rechargeable Batteries. *Electrochem. Solid-State Lett.* **1999**, *2*, 547−549.
(5) Kasavajjula, U.; Wang, C.; Appleby, A. J. Nano- and Bulk-silicon-based Insertion Anodes for Lithium-ion Secondary Cells. *J. Power Sources* **2007**, *163*, 1003−1039.
(6) Liu, X. H.; Zhong, L.; Huang, S.; Mao, S. X.; Zhu, T.; Huang, J. Y. Size-Dependent Fracture of Silicon Nanoparticles During Lithiation. *ACS Nano* **2012**, *6*, 1522−1531.
(7) Zhu, J.; Gladden, C.; Liu, N.; Cui, Y.; Zhang, X. Nanoporous Silicon Networks as Anodes for Lithium Ion Batteries. *Phys. Chem. Chem. Phys.* **2013**, *15*, 440−443.
(8) Chan, C. K.; Peng, H.; Liu, G.; McIlwrath, K.; Zhang, X. F.; Huggins, R. A.; Cui, Y. High-performance Lithium Battery Anodes using Silicon Nanowires. *Nat. Nanotechnol.* **2008**, *3*, 31−35.
(9) Liu, N.; Wu, H.; McDowell, M. T.; Yao, Y.; Wang, C.; Cui, Y. A Yolk-Shell Design for Stabilized and Scalable Li-Ion Battery Alloy Anodes. *Nano Lett.* **2012**, *12*, 3315−3321.
(10) Chen, S.; Gordin, M. L.; Yi, R.; Howlett, G.; Sohn, H.; Wang, D. Silicon Core-hollow Carbon Shell Nanocomposites with Tunable Buffer Voids for High Capacity Anodes of Lithium-ion Batteries. *Phys. Chem. Chem. Phys.* **2012**, *14*, 12741−12745.
(11) Wu, H.; Chan, G.; Choi, J. W.; Ryu, I.; Yao, Y.; McDowell, M. T.; Lee, S. W.; Jackson, A.; Yang, Y.; Hu, L.; Cui, Y. Stable Cycling of Double-walled Silicon Nanotube Battery Anodes Through Solid-electrolyte Interphase Control. *Nat. Nanotechnol.* **2012**, *7*, 310−315.
(12) Zhang, T.; Gao, J.; Fu, L. J.; Yang, L. C.; Wu, Y. P.; Wu, H. Q. Natural Graphite Coated by Si Nanoparticles as Anode Materials for Lithium Ion Batteries. *J. Mater. Chem.* **2007**, *17*, 1321−1325.
(13) Liu, Y.; Qiu, X.; Guo, X. Improving Coulombic Efficiency by Confinement of Solid Electrolyte Interphase Film in Pores of Silicon/carbon Composite. *J. Mater. Chem. A* **2013**, *1*, 14075−14079.
(14) Martin, C.; Alias, M.; Christien, F.; Crosnier, O.; Bélanger, D.; Brousse, T. Graphite-Grafted Silicon Nanocomposite as a Negative Electrode for Lithium-Ion Batteries. *Adv. Mater.* **2009**, *21*, 4735−4741.
(15) Yi, R.; Zai, J.; Dai, F.; Gordin, M. L.; Wang, D. Improved Rate Capability of Si−C Composite Anodes by Boron Doping for Lithium-ion Batteries. *Electrochem. Commun.* **2013**, *36*, 29−32.
(16) Martin, C.; Crosnier, O.; Retoux, R.; Bélanger, D.; Schleich, D. M.; Brousse, T. Chemical Coupling of Carbon Nanotubes and Silicon Nanoparticles for Improved Negative Electrode Performance in Lithium-Ion Batteries. *Adv. Funct. Mater.* **2011**, *21*, 3524−3530.
(17) Wu, H.; Yu, G.; Pan, L.; Liu, N.; McDowell, M. T.; Bao, Z.; Cui, Y. Stable Li-ion Battery Anodes by In-situ Polymerization of Conducting Hydrogel to Conformally Coat Silicon Nanoparticles. *Nat. Commun.* **2013**, *4*.
(18) Lee, J. K.; Smith, K. B.; Hayner, C. M.; Kung, H. H. Silicon Nanoparticles-graphene Paper Composites for Li ion Battery Anodes. *Chem. Commun.* **2010**, *46*, 2025−2027.
(19) Zhou, X.; Yin, Y.-X.; Wan, L.-J.; Guo, Y.-G. Facile Synthesis of Silicon Nanoparticles Inserted into Graphene Sheets as Improved Anode Materials for Lithium-ion Batteries. *Chem. Commun.* **2012**, *48*, 2198−2200.
(20) Luo, J.; Zhao, X.; Wu, J.; Jang, H. D.; Kung, H. H.; Huang, J. Crumpled Graphene-Encapsulated Si Nanoparticles for Lithium Ion Battery Anodes. *J. Phys. Chem. Lett.* **2012**, *3*, 1824−1829.
(21) Chou, S.-L.; Wang, J.-Z.; Choucair, M.; Liu, H.-K.; Stride, J. A.; Dou, S.-X. Enhanced Reversible Lithium Storage in a Nanosize Silicon/graphene Composite. *Electrochem. Commun.* **2010**, *12*, 303−306.
(22) Wen, Y.; Zhu, Y.; Langrock, A.; Manivannan, A.; Ehrman, S. H.; Wang, C. Graphene-Bonded and -Encapsulated Si Nanoparticles for Lithium Ion Battery Anodes. *Small* **2013**, *9*, 2810−2816.
(23) Xun, S.; Song, X.; Wang, L.; Grass, M. E.; Liu, Z.; Battaglia, V. S.; Liu, G. The Effects of Native Oxide Surface Layer on the Electrochemical Performance of Si Nanoparticle-Based Electrodes. *J. Electrochem. Soc.* **2011**, *158*, A1260−A1266.
(24) Yu, B.-C.; Hwa, Y.; Park, C.-M.; Kim, J.-H.; Sohn, H.-J. Effect of Oxide Layer Thickness to Nano-Si Anode for Li-ion Batteries. *RSC Adv.* **2013**, *3*, 9408−9413.
(25) Hu, Y.-S.; Demir-Cakan, R.; Titirici, M.-M.; Müller, J.-O.; Schlögl, R.; Antonietti, M.; Maier, J. Superior Storage Performance of a Si@SiOx/C Nanocomposite as Anode Material for Lithium-Ion Batteries. *Angew. Chem., Int. Ed.* **2008**, *47*, 1645−1649.
(26) Li, Z.-F.; Zhang, H.; Liu, Q.; Liu, Y.; Stanciu, L.; Xie, J. Covalently-grafted Polyaniline on Graphene Oxide Sheets for High Performance Electrochemical Supercapacitors. *Carbon* **2014**, *71*, 257−267.
(27) Li, X.; He, Y.; Swihart, M. T. Surface Functionalization of Silicon Nanoparticles Produced by Laser-Driven Pyrolysis of Silane followed by HF−HNO3 Etching. *Langmuir* **2004**, *20*, 4720−4727.
(28) Hui, C. M.; Pietrasik, J.; Schmitt, M.; Mahoney, C.; Choi, J.; Bockstaller, M. R.; Matyjaszewski, K. Surface-Initiated Polymerization as an Enabling Tool for Multifunctional (Nano-)Engineered Hybrid Materials. *Chem. Mater.* **2013**, *26*, 745−762.
(29) Sakellariou, G.; Priftis, D.; Baskaran, D. Surface-initiated Polymerization from Carbon Nanotubes: Strategies and Perspectives. *Chem. Soc. Rev.* **2013**, *42*, 677−704.
(30) Kim, C.; Fujino, T.; Miyashita, K.; Hayashi, T.; Endo, M.; Dresselhaus, M. S. Microstructure and Electrochemical Properties of Boron - Doped Mesocarbon Microbeads. *J. Electrochem. Soc.* **2000**, *147*, 1257−1264.
(31) Magasinski, A.; Zdyrko, B.; Kovalenko, I.; Hertzberg, B.; Burtovyy, R.; Huebner, C. F.; Fuller, T. F.; Luzinov, I.; Yushin, G. Toward Efficient Binders for Li-Ion Battery Si-Based Anodes: Polyacrylic Acid. *ACS Appl. Mater. Interfaces* **2010**, *2*, 3004−3010.